Ru, Pd doped WO3 nanomaterials: A synergistic effect of noble metals to enhance the acetone response properties

Article *in* Ceramics International · March 2022

DOI: 10.1016/j.ceramint.2022.03.065

CITATIONS
13

READS
227

7 authors, including:

Pandurang A. Ghadage
Punyashlok Ahilyadevi Holkar Solapur University Solapur
9 PUBLICATIONS **25** CITATIONS
SEE PROFILE

Digambar Nadargi
Center For Materials For Electronics Technology (C-MET)
54 PUBLICATIONS **2,291** CITATIONS
SEE PROFILE

Kiran Shinde
Hanbat National University
43 PUBLICATIONS **302** CITATIONS
SEE PROFILE

Imtiaz S. Mulla
CSIR - National Chemical Laboratory, Pune
230 PUBLICATIONS **7,484** CITATIONS
SEE PROFILE

Ceramics International 48 (2022) 17923–17933

Contents lists available at ScienceDirect

Ceramics International

journal homepage: www.elsevier.com/locate/ceramint

Ru, Pd doped WO_3 nanomaterials: A synergistic effect of noble metals to enhance the acetone response properties

Pavan M. Kodam [a], Pandurang A. Ghadage [a], Digambar Y. Nadargi [a,*], K.P. Shinde [b], Imtiaz S. Mulla [c], J.S. Park [b,**], Sharad S. Suryavanshi [a,***]

[a] School of Physical Sciences, PAH Solapur University, Solapur, 413255, M.S, India
[b] Department of Materials Science and Engineering, Hanbat National University, Daejeon, 34158, South Korea
[c] Former Emeritus Scientist, NCL, Pune, 411008, M.S, India

ARTICLE INFO

Keywords:
Synergistic effect
WO_3
Ru–Pd doping
Precipitation route
Acetone vapours

ABSTRACT

Noble metals (NMs) have an enormous impact on the intrinsic properties of the metal oxides. We report the synergistic effect of Ruthenium (Ru) and Palladium (Pd) noble metals on the enhancement of gas sensing properties of pure tungsten oxide (WO_3). The gas sensing material is synthesized by simple and straight forward precipitation route, and its physico-chemical analyses are determined using XRD, FESEM, TEM/HRTEM, FFT, UV–Vis, XPS, EDAX, and BET measurements. Use of the developed material as a gas sensor is evaluated using several target gases (oxidizing as well as reducing), with acetone showing the best selectivity. The noble metal doping and hence catalytic action improved the gas response qualities. The synergistic effect of Ru and Pd on WO_3 gas response properties are identified, where the effect is 99.80% sensitivity, and lower response/recovery time (10 s and 2 min) at 300 °C operating temperature. Nonetheless, the sensors displayed better gas sensing properties even at lower operating temperatures ranging from 200 to 275 °C. In addition, the synergistic effect has displayed the dramatic enhancement in the sensitivity to 76.44% at barely 10 ppm acetone concentration. This particular result will undoubtedly be helpful for diagnostic purpose of diabetic patients, and a strong candidate for prospective gas sensing applications, particularly acetone.

1. Introduction

Human life is surrounded by various metal oxides that are being used in the diverse array of applications. With the time, the metal oxides deteriorate due to various environmental conditions such as humid atmosphere, temperature, and aging. An incorporation of noble metals, not only protect from the corrosion/oxidation/aging effect, but also improve the properties of the metal oxides. The periodic table elements from 44 to 47 (ruthenium-Ru, rhodium-Rh, palladium-Pd, silver-Ag) and 76 to 79 (osmium-Os, iridium-Ir, platinum-Pt, gold-Au) are referred as noble metals (Fig. 1). The NMs namely Pd, Pt, and Rh have the potential applications in automotive industries such as catalysts or catalytic converters [1]. Similarly, the electronic industry comprising of smartphones, computers and laptops utilises Ag, Au, Pt, Pd noble metals for various particular purpose [2–5]. There are other sectors such as photocatalysis [6], fuel cells [7], and gas sensors [8], where the noble metals play a crucial role in enhancing their efficiency. In the gas sensors, noble metals trigger the spillover mechanism as well as acts as catalyst for improving the gas response properties of the metal oxide.

In the state-of-art, the research groups are actively engaged in developing the noble metal incorporated metal oxide based gas sensors. Mulla et al. have developed tin oxide gas sensors using Pd and Ru noble metals to enhance the hydrogen gas response [9]. Yao et al. studied WO_3 nanowire bundles for gas sensing application by using bimetals Au-Pd [10]. Li et al. have demonstrated AuPd nanoparticles modified SnO_2 for enhanced -acetone and -formaldehyde response due to the synergistic effect of bimetallic nanoparticles [11].

However, there are minimal reports available, where the gas sensitivity as well as response/recovery time can be tuned synergistically, using two different NMs, individually. To the best of our knowledge, no reports are available that disseminate the results on enhancing the gas sensitivity and at the same time, minimising the response/recovery time

* Corresponding author.
** Corresponding author.
*** Corresponding author.
E-mail addresses: digambar_nadargi@yahoo.co.in (D.Y. Nadargi), jsphb@hanbat.ac.kr (J.S. Park), sssuryavanshi@rediffmail.com (S.S. Suryavanshi).

https://doi.org/10.1016/j.ceramint.2022.03.065
Received 5 January 2022; Received in revised form 2 March 2022; Accepted 6 March 2022
Available online 12 March 2022

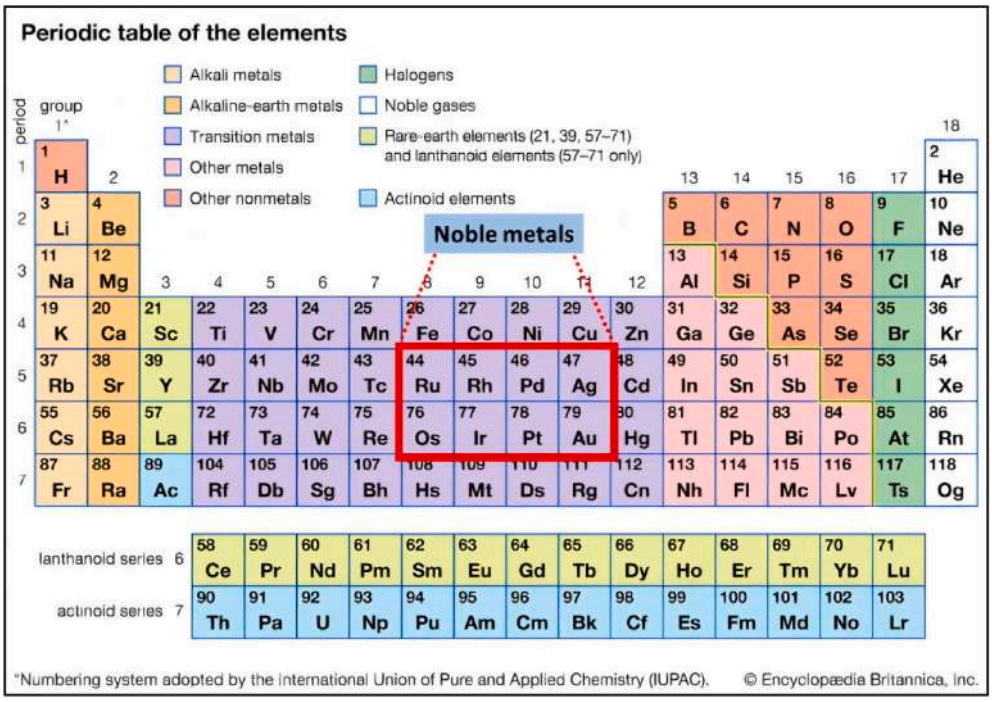

Fig. 1. Periodic table highlighting Noble metals, CC Encyclopaedia Britannica, Inc.

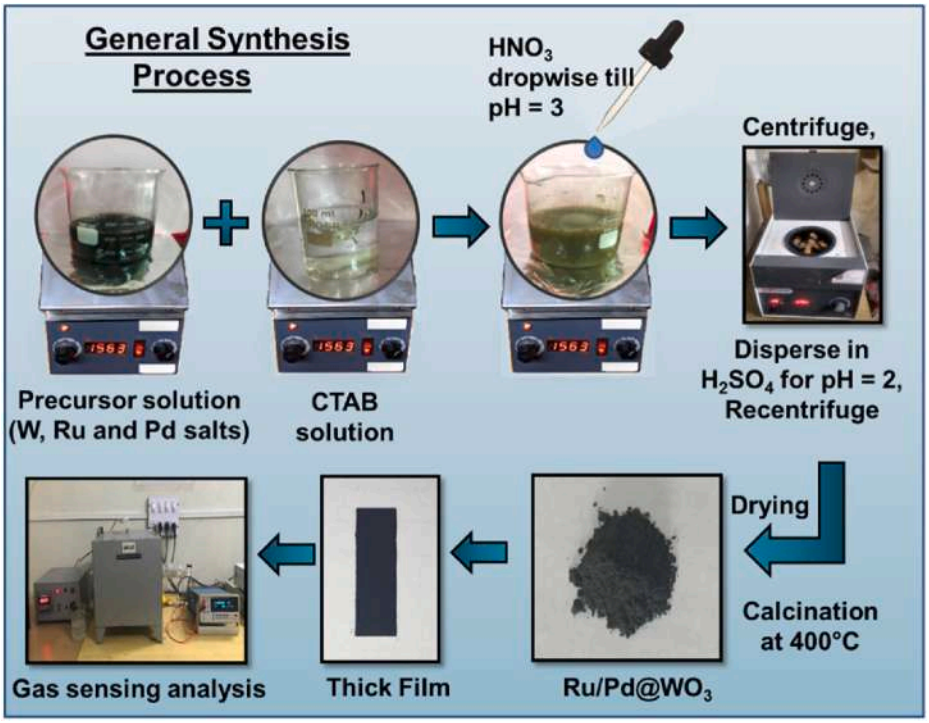

Scheme 1. Typical synthesis process by precipitation route.

of the parent metal oxide. With this motivation, the efforts were made to elucidate the synergism between Ru and Pd to enhance the WO_3 response towards acetone vapours. The reason behind choosing the WO_3 metal oxide semiconductor is due to its wide band gap (2.4–2.8 eV), better physical and chemical stability in the harsh environment, and cost effectiveness [12]. Formally, acetone is the most explored target gas for chemiresistive gas sensors, due to its potential impact on human health [13]. For the rapid diagnosis of diabetic patients, acetone concentration in ppb/ppm levels in the respiration system acts as a biomarker [14].

In the present work, the efforts were made to study the synergistic effect of Ru and Pd on WO_3 to (i) enhance the acetone sensitivity, and (ii) minimise the response/recovery time. The gas sensing parameters were systematically investigated by tuning the noble metals (Ru and Pd) in the WO_3.

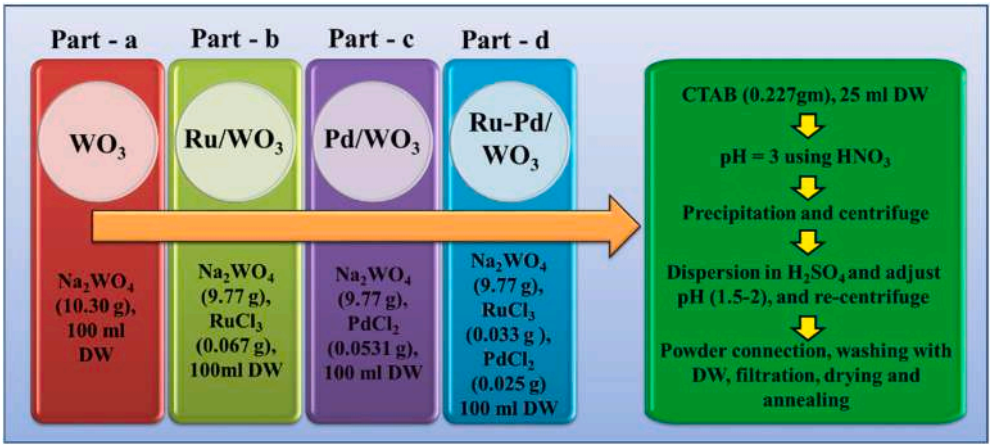

Scheme 2. Flowchart of material synthesis protocol.

Step 1: Protonation

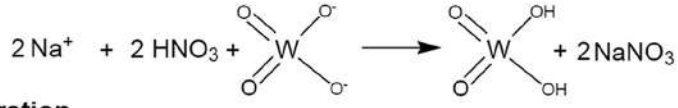

Step 2: Hydration

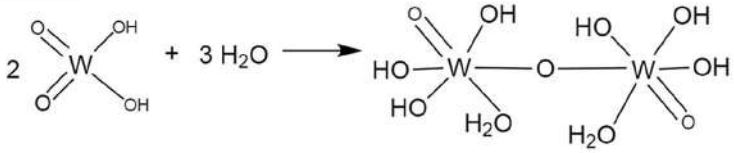

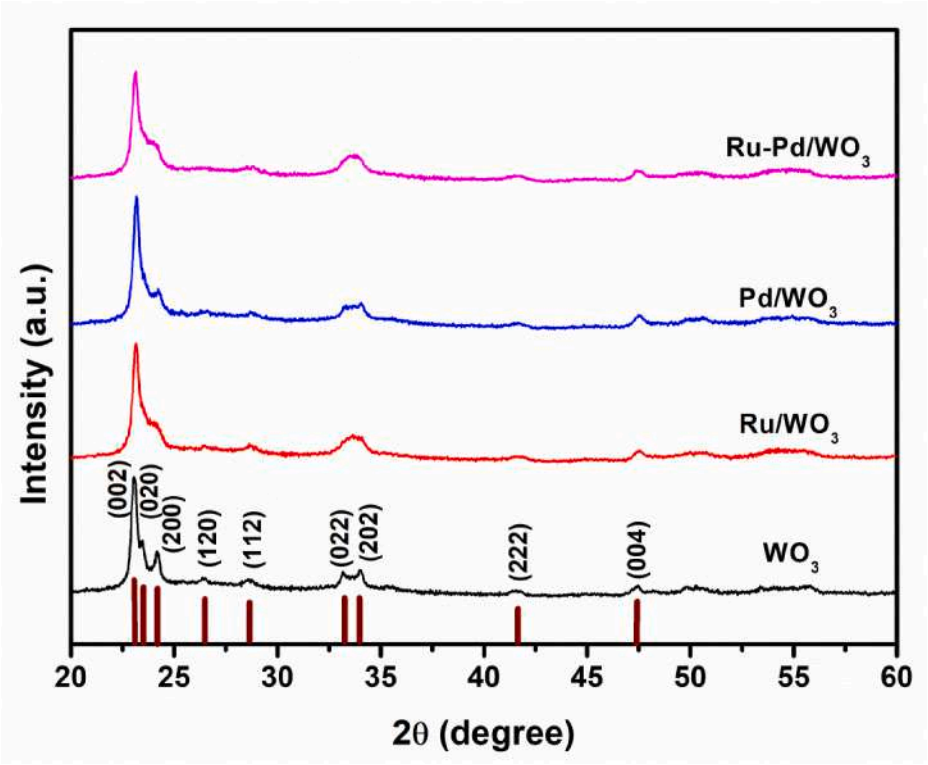

Fig. 2. XRD pattern of pristine WO_3 and Ru, Pd, Ru–Pd doped WO_3 by precipitation route.

Table 1
Crystallite size and Lattice parameters of the developed samples.

Sample Code	Crystallite Size (nm)	Lattice Parameters (Å)
WO_3	21.20	a = 7.29, b = 7.53, c = 7.68 (a≠b≠c)
Pd/WO_3	20.49	
Ru/WO_3	13.62	
$Ru–Pd/WO_3$	12.17	

2. Experimental procedure

In general, a facile precipitation route was adopted to develop the Ru/Pd doped WO_3 nanomaterials. In a typical experiment (Scheme 1), the precursor solution was prepared in an appropriate molar concentration of the metal salts using distilled water (DW). The precipitation was obtained by means of HNO_3 as well as H_2SO_4 acids at certain pH values. Four different types of samples are discussed in this work: (a) pristine tungsten oxide, (b) Ru doped tungsten oxide, (c) Pd doped tungsten oxide, and (d) Ru–Pd doped tungsten oxide (Scheme 2).

In part (a), pristine tungsten oxide was prepared by dissolving sodium tungstate dihydrate ($Na_2WO_4{\cdot}2H_2O$ S.D. Fine-Chem limited AR grade) of 10.30 g (30 mmol) in 100 mL distilled water. In a separate beaker, cetyltrimethylammonium bromide ($C_{19}H_{42}BrN$, Sigma Aldrich AR grade) of 0.23 g (0.62 mmol) was dissolved in 25 mL distilled water. The as-prepared CTAB solution was then transferred to the precursor solution. The precipitation process was triggered by using drop-wise addition of HNO_3 till the pH attains 3. The obtained green precipitate was then centrifuged at 2000 rpm for 5 min. After decanting the supernatant, the precipitate was dissolved back into H_2SO_4 till the pH attains 2. The as-obtained final precipitate was then washed with an ample amount of distilled water, and re-centrifuged at 2000 rpm for 5 min. The precipitate was dried at room temperature, followed by annealing at 400 °C for 2 h. In a similar way, part b and c were carried out by replacing an amount of ammonium tungstate corresponding to 1 mol% (doping level) of both the noble metals (Ruthenium (III) chloride hydrate ($RuCl_3{\cdot}H_2O$), Palladium (II) chloride ($PdCl_2$), Sigma Aldrich AR grade), respectively.

However, for synergistic effect, part d was carried out by taking 0.5 mol% of each noble metals, to get the sum of 1 mol%. The as-sintered oxide powders were used to fabricate the thick films. The details of thick film fabrication, characterisations and gas sensing measurements of the samples are explained in the supplementary section, so as to have a room to discuss the main results. In the present acid mediated precipitation route, the reaction during the formation of pristine WO_3 occurs in two major steps. *Step 1:* Protonation of the tungstate ions upon acidification of solution to form solid precipitates, followed by *Step 2:* Hydration of the $[WO_2(OH)_2]$ tetrahedral molecules and dimerization via O-bridging to form crystalline $[WO(OH)_3(H_2O)]_2(\mu\text{-}O)$ containing octahedral W-centres.

3. Results and discussion

3.1. XRD analysis

XRD analysis of pristine and Ru/Pd doped WO_3 was carried out by using grazing incidence X-ray diffraction (XRD). The corresponding XRD signatures along with the reference WO_3 are shown in Fig. 2. All the samples exhibited a characteristic monoclinic crystal structure that corresponds well to the Bragg reflections of the JCPDS reference (43–1035) [15]. The corresponding planes associated with monoclinic structure of WO_3 are: (002), (020), (200), (120), (112), (022), (202) (222), and (004).

The values for the d-spacing and average lattice parameters are calculated by considering the FWHM of the most intense peak (002), using Scherrer formula [16], and tabulated in Table 1.

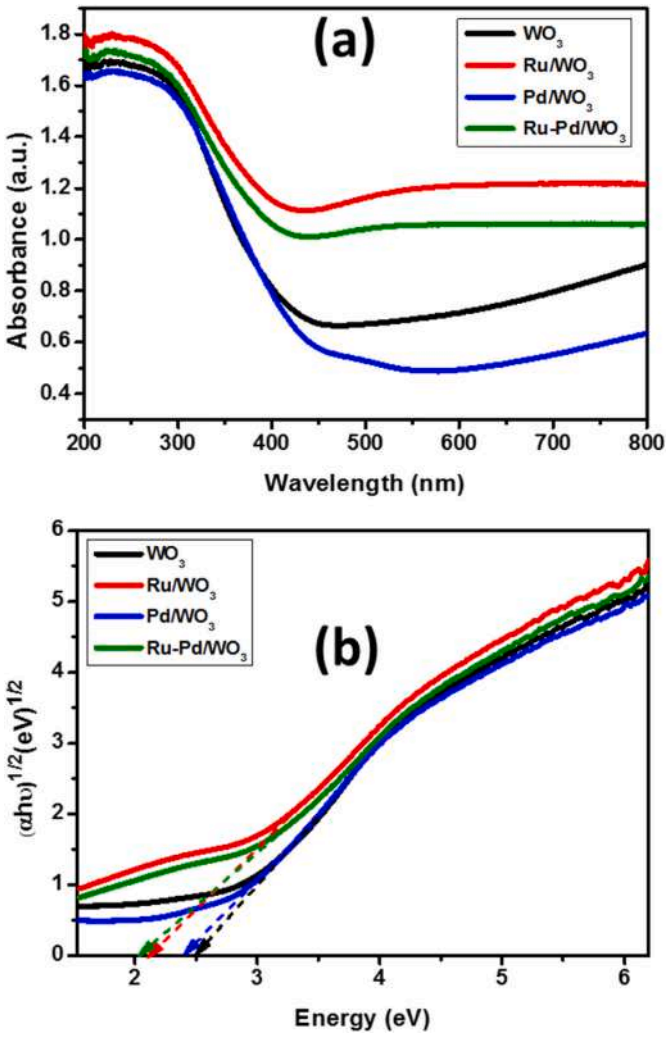

Fig. 3. UV–Visible spectra of Pristine WO_3, Ru/WO_3, Pd/WO_3, $Ru–Pd/WO_3$: a) Absorbance spectra, and b) Band gap energy.

$$D = \frac{K\,\lambda}{\beta\ cos\ \theta} \tag{1}$$

where, D = Average crystal diameter, β = FWHM, K = constant related to the shape of the crystallites (K = 0.89), λ = wavelength of the X-rays, and θ = diffraction angle.

As expected, the crystallite size of the pristine WO_3 got decreased upon doping of both noble metals (Ru and Pd), which helped to enhance the surface area, thereby gas sensing properties.

3.2. UV–Visible spectroscopy analysis

The UV–Visible absorbance spectra of pure and noble metal doped WO_3 are shown in Fig. 3. a. UV-Vis absorption of the produced nanoparticles begins at 450 nm (for pristine WO_3), 427 nm (for Ru/WO_3), 485 nm (for Pd/WO_3), and 417 nm (for $Ru–Pd/WO_3$). Furthermore, the band gaps for pure WO_3, Ru/WO_3, Pd/WO_3, and $Ru–Pd/WO_3$ were determined to be 2.49 eV, 2.12 eV, 2.40 eV, and 2.03 eV, respectively.

Tauc's relation was used to determine the band gap energy of the samples and is given by,

$$\alpha = C \times \frac{(h\nu - E_g)^n}{h\nu} \tag{2}$$

where, E_g is the optical band gap energy which was calculated from

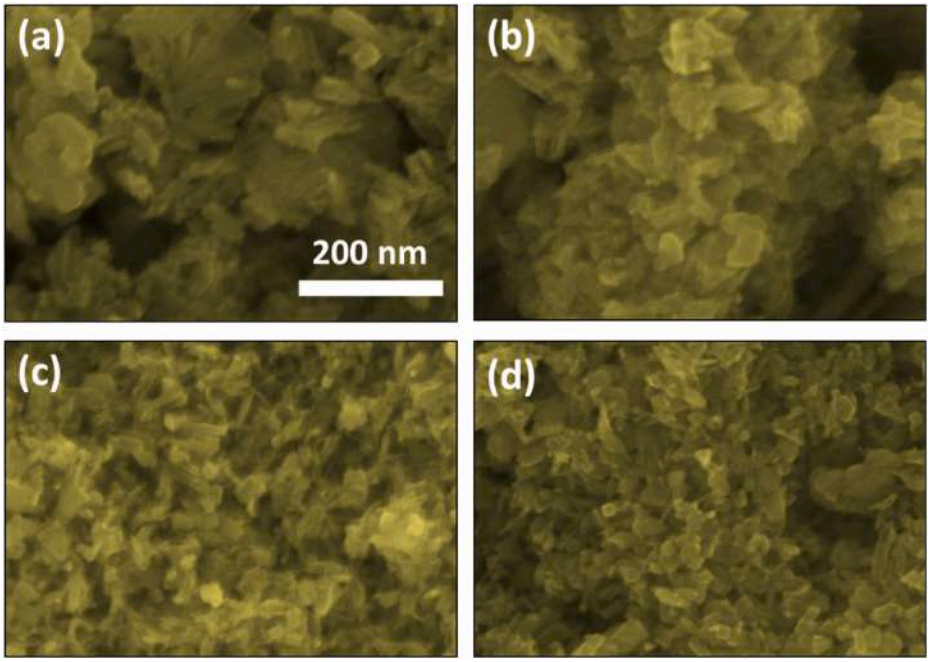

Fig. 4. FESEM images of - a) pristine WO_3, b) Pd/WO_3, c) Ru/WO_3, and d) $Ru–Pd/WO_3$.

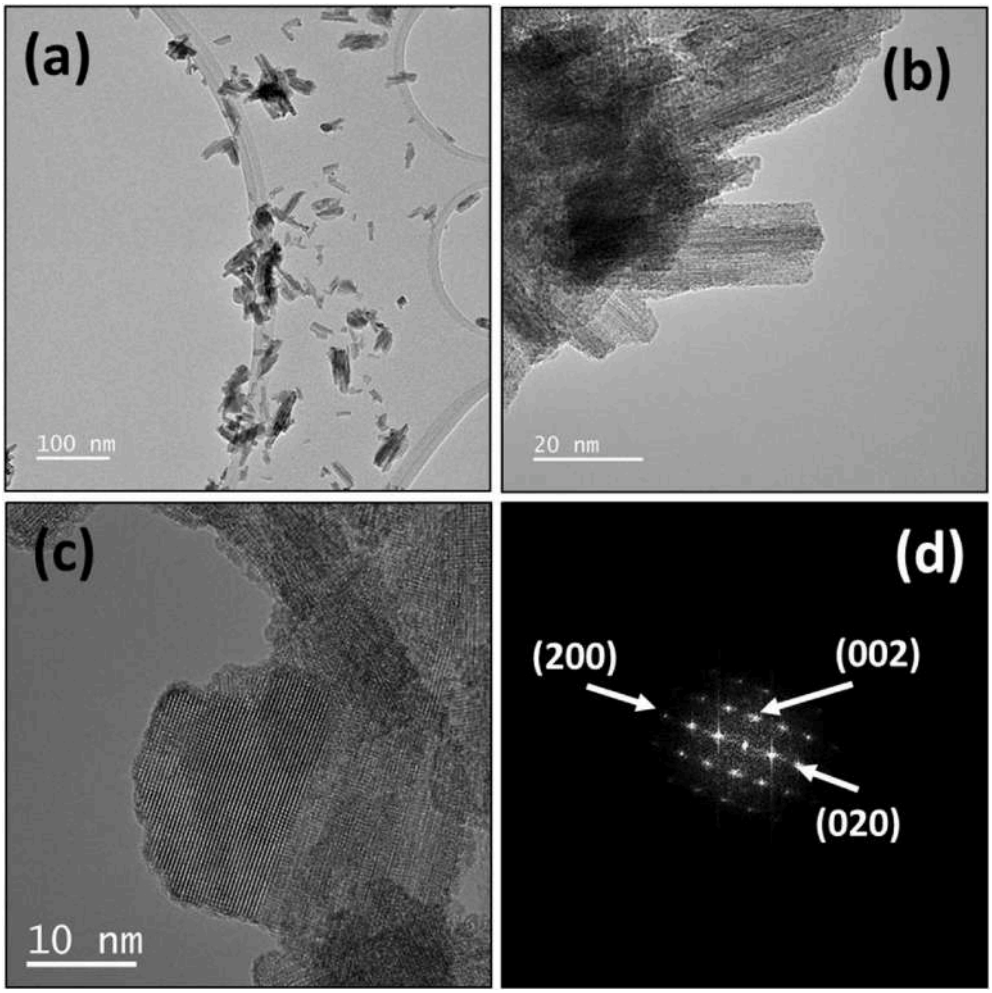

Fig. 5. TEM (a, b), HRTEM (c), and FFT (d) images of Ru–Pd doped WO_3.

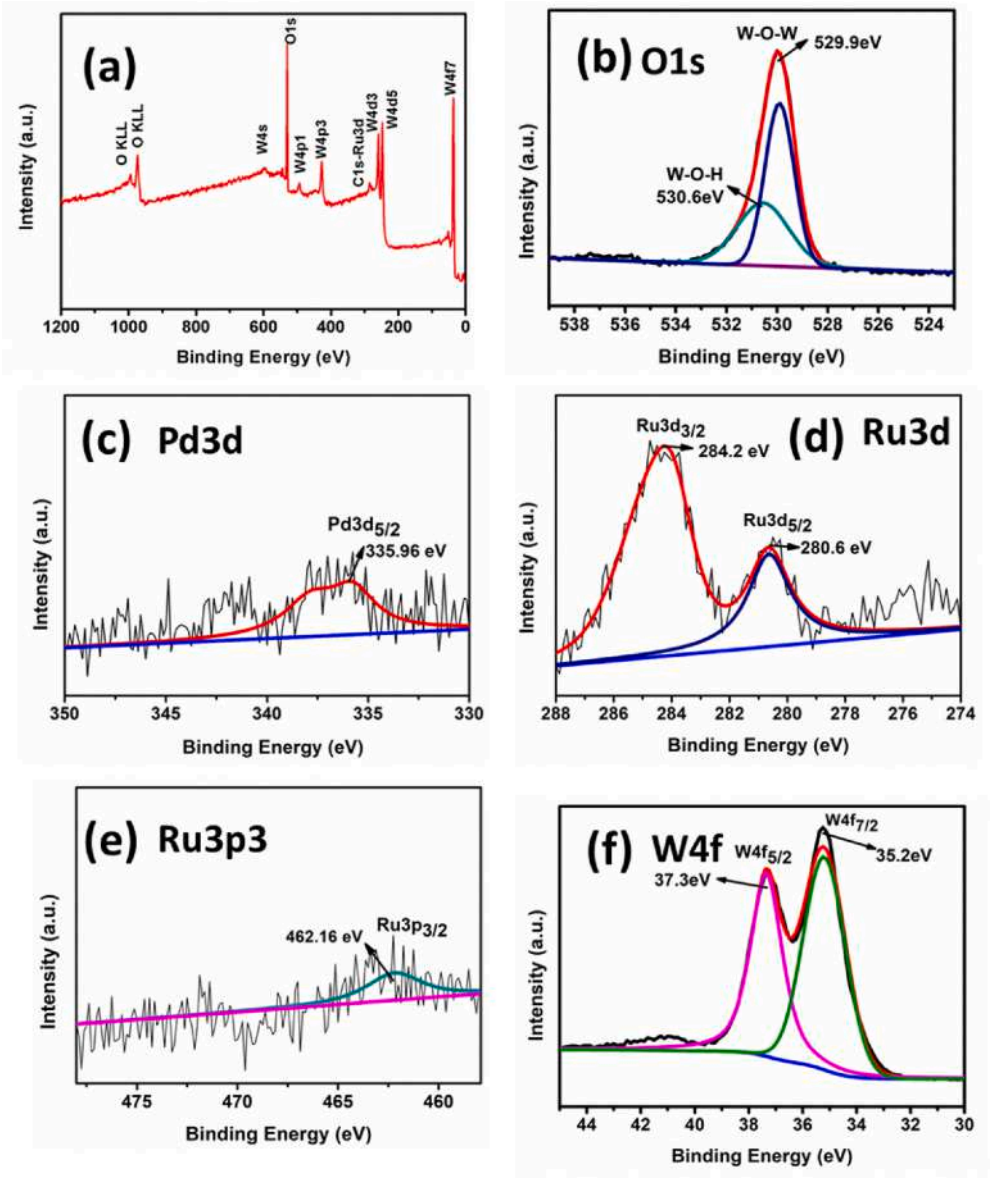

Fig. 6. XPS spectra of optimised Ru–Pd doped WO_3 sample.

$(\alpha h\nu)^2$ versus energy ($h\nu$) plot, α is the absorption coefficient and $h\nu$ is the photon energy taken from the UV-spectra. The band edge can be estimated from the intercept of the extrapolated linear part ($\alpha = 0$) of the curve on energy axis.

The band gap values of pure and Pd doped WO_3 were found to be greater than those of Ru and Ru–Pd doped WO_3. The noble metals (Ru–Pd) doped WO_3 sample shows the lowest bandgap of 2.03 eV. It clearly indicates the synergistic effect in WO_3, showing the strongest acetone response qualities compared to the other samples in the set.

3.3. FESEM, TEM and FFT analyses

Morphological studies of the developed samples were accomplished by FESEM analysis. Fig. 4(a–d) and Figure S1 (a-d) show FESEM images of pristine and noble metal doped WO_3 at two different magnification levels (200 nm and 500 nm). From the images, it is clearly seen that the slit-like grains of 193.5 nm, 322 nm, 107 nm and 91.37 nm size are obtained, confirming the formation of nanomaterials. On visual inspection, the grain size of pristine WO_3 (Fig. 4a) and Pd/WO_3 (Fig. 4b) are higher, as compared to Ru/WO_3 (Fig. 4c) and Ru–Pd/WO_3 (Fig. 4d). The clusters of grains are seen in case of pristine and Pd doped WO_3, whereas smaller and individual grains are visible in case of Ru/WO_3 and Ru–Pd/WO_3. The least grain size is obtained for Ru–Pd/WO_3 nanomaterial (91.37 nm), which indicate the better gas response properties (discussed later in the gas sensing analysis part). In general, the bunch of these slits make the nanomaterial more porous, and yielding the high surface area, needed for better gas response properties (response and recovery time) by easy adsorption and desorption of the oxygen molecules on the sensor surface. Similarly, looking at zoomed magnification images (Figure S1a-d), empty spaces and voids are present in the samples. The slit-like morphology is further revealed from BET analysis, which is discussed in the later section.

Fig. 5 showcase the TEM/HRTEM images of Ru–Pd doped WO_3 sample along with the Fast Fourier Transform (FFT) image. In correlation with the FESEM studies, the slit-like structures (rather slits) are clearly visible in the TEM images (Fig. 5 a & b). The higher magnified TEM image (Fig. 5b) displays the oriented attachment of numerous slits together to form the close packed structure. HRTEM images show the identical diffraction pattern, verifying the crystal structure study performed using XRD. The (002), (020), and (200) planes are represented

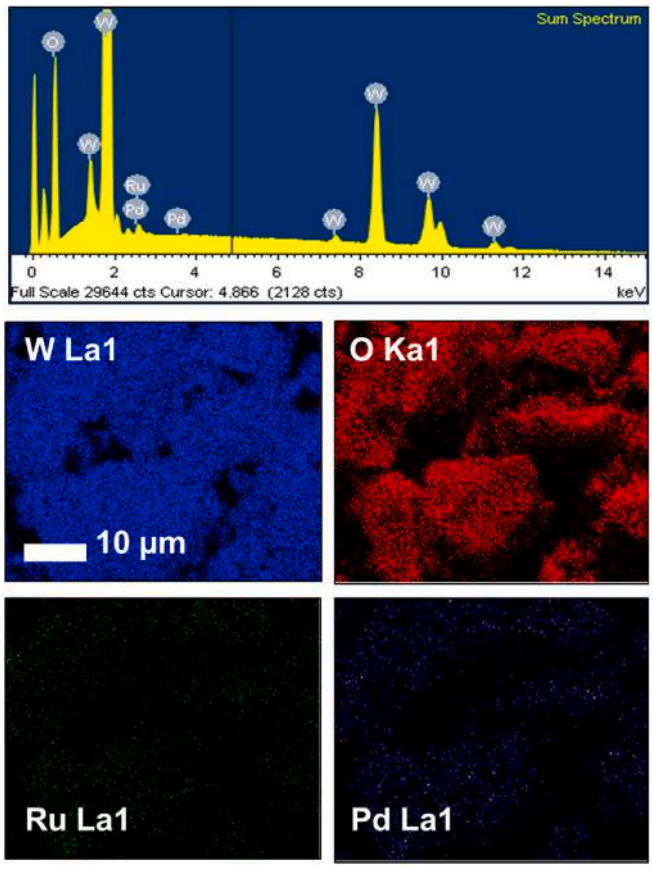

Fig. 7. EDAX spectrum and elemental mapping of Ru–Pd doped WO_3.

by the indexed locations in the Fast Fourier Transform (FFT) patterns, indicating the monoclinic phase WO_3 nano-slits, with a single crystalline property.

3.4. XPS and EDAX analyses

The XPS technique was used to identify the oxidation states of different elements on the surface of Ru–Pd doped WO_3. Fig. 6 shows the survey spectrum as well as the associated deconvoluted spectra of each constituent elements. The survey spectrum (Fig. 6a) demonstrates the existence of O1s, Pd3d, Ru3d, Ru3p3 and W4f at their respective binding energy values. The peak at 529.9 eV in the O1s spectrum (Fig. 6b) corresponds to W–*O*–W bond, and the shoulder peak at 530.6 eV is due to surface contamination by hydroxyl groups [17]. Pd $3d_{5/2}$ is responsible for the spin-orbital binding energy peaks of Pd3d (Fig. 6c) suggesting the presence of Pd^{2+} oxidation state. Ru3d XPS peaks shown in (Fig. 6d), have two humps at 284.2 eV and 280.6 eV assigned to $Ru3d_{3/2}$ and $Ru3d_{5/2}$, respectively [18]. In addition, Ru3p3 spectrum (Fig. 6e) showcase $Ru3p_{3/2}$ at 462.31 eV suggesting the presence of Ru^{3+} oxidation state. The presence of W^{6+} oxidation state was confirmed by the emergence of W $4f_{7/2}$ (35.2 eV) and W $4f_{5/2}$ (37.3 eV) peaks [19,20]. The spin orbit components of $W4f_{7/2}$ and $W4f_{5/2}$ are well separated, with an energy separation of 2.17 eV [21].

In Fig. 7, energy dispersive X-ray (EDAX) spectrum along with the elemental mapping are represented. The EDAX spectrum revealed all the elements of Ru–Pd functionalized WO_3. These elements (W, O, Ru, and Pd) are further mapped to check the uniform distribution of the noble metals (Ru and Pd) in the parent metal oxide. They seem to be uniformly distributed successfully across the WO_3 matrix. The homogenous distribution of these elements in atomic % are: O = 79.78%, Ru = 0.65%, Pd = 0.15%, and W = 19.42%.

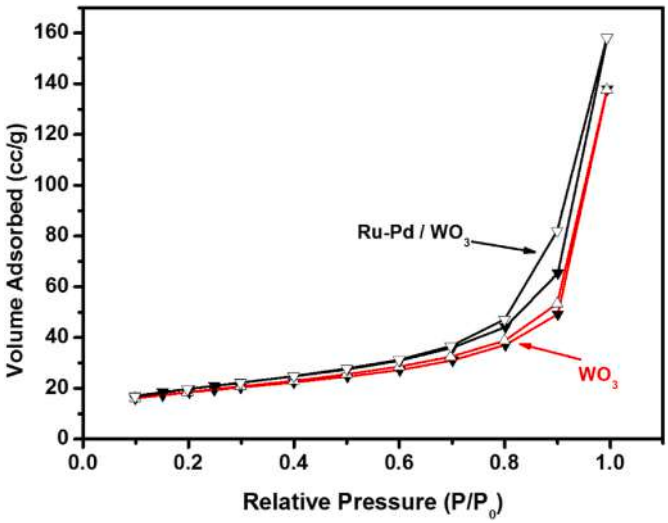

Fig. 8. N_2 adsorption and desorption isotherms of pristine and Ru–Pd doped WO_3.

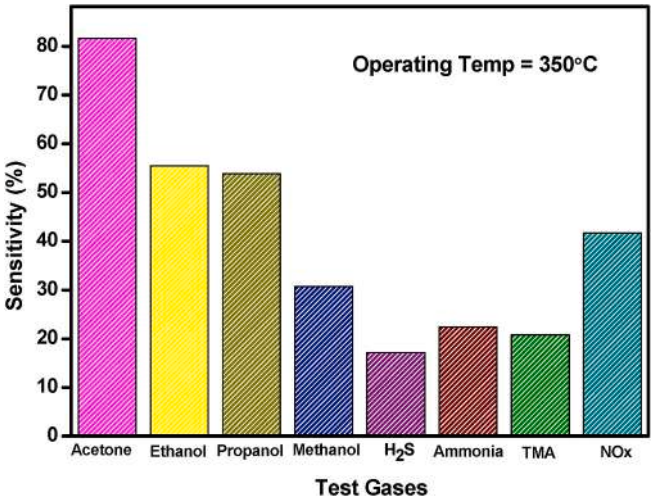

Fig. 9. Gas selectivity of WO_3 sensor for gases.

3.5. BET analysis

Pristine WO_3 and Ru–Pd/WO_3 were analyzed with BET surface area analyser. The adsorption and desorption of N_2 gas showed a hysteresis loop in the range of 0.1–1.0 relative pressure (P/P_0) as shown in Fig. 8. According to the IUPAC classification, the synthesized pristine WO_3 and Ru–Pd/WO_3 hysteresis loops show a type IV isotherm with the form H_3 loop-type, indicating a mesoporous and slit-like structure [22]. Furthermore, the surface area of Ru–Pd doped WO_3 (68.39 m^2/g) was obtained to be higher than pristine WO_3 (62.12 m^2/g), indicating the better gas sensing properties upon noble metal doping [23].

3.6. Gas sensing analysis

First of all, the sensing capability of pristine WO_3 towards several reducing as well as oxidizing gases such as ammonia, trimethylamine (TMA), acetone, alcohols (methanol, ethanol, and propanol), hydrogen sulphide (H_2S), and nitrous oxide (NO_x) is explored in detail. Pristine WO_3 showed the highest selectivity towards acetone vapours, when compared to the other test gases (Fig. 9). Its response value (S%) hits 83% at 500 ppm acetone concentration with an operating temperature of 350 °C. In addition, alcohol family exhibited a discernible response

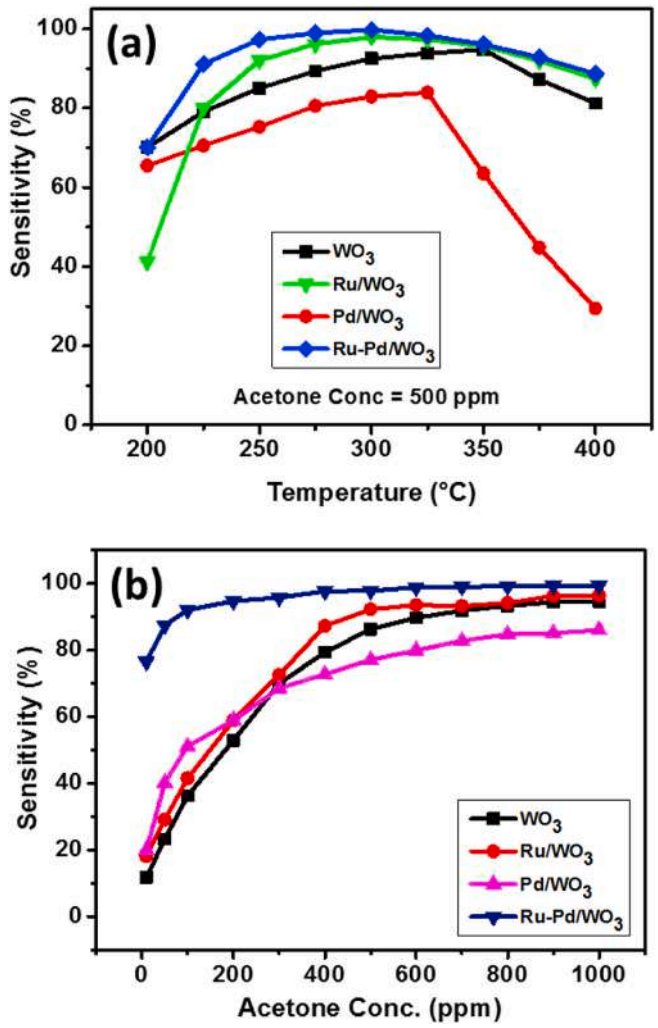

Fig. 10. (a) Sensitivity as a function of operating temperature, and b) sensitivity as a function of acetone concentration.

(methanol: 30.69%, ethanol: 55.51%, and propanol: 53.84%) at the same operating temperature (350 °C) and at 500 ppm analytes concentration. In contrast, for strong odor gases such H_2S, ammonia, and TMA, the sensor showed the response as 17.16%, 22.40%, and 20.80%, respectively at 100 ppm gas concentration. The gas response of sensor for these gases at their 100 ppm concentrations is reported, because at higher concentrations they blocked the sensor. To be more precise, the sensor material did not show any recovery, when higher concentration (500 ppm) of H_2S, ammonia, and TMA gas were injected. Therefore, comparing the sensor response at 100 ppm concentration of the highest responded gas (i.e. acetone vapours), the sensitivity is obtained to be 36.31% (Fig. S2). For the oxidizing gas, NO_x, sensor displayed almost similar response (41.69%) as of ethanol and propanol, at the same operating temperature (350 °C) and at 500 ppm concentration. Keeping in view of acetone selectivity, the other gas response properties of pristine WO_3 and thereby noble metal doped WO_3, were systematically investigated.

As shown in Fig. 10. a, the sensors response towards acetone vapours (500 ppm) varies as the working temperature increases from 200 °C to 400 °C. As the temperature rise, the resistance of the sensor went down, which meant it is n-type semiconductor [24]. Sensors made of pure WO_3, and Ru, Pd, and Ru–Pd doped WO_3 were displayed similar curves over a wide range of temperature. Initially, the gas response went up with the temperature, reached a certain point, and then went down with the increasing temperature [25,26]. Pristine WO_3 showed the sensitivity

Table 2
Gas sensing analysis of as developed pristine and noble metal doped WO_3 in details.

Sr. No	Sample	Optimum Operating Temp (°C)	Response Time	Recovery Time	S (%)
1	WO_3	350	15 s	3 min 30 s	94.81
2	Ru/WO_3	300	1 min	3 min 50 s	98.01
3	Pd/WO_3	325	10 s	2 min 30 s	83.96
4	Ru–Pd/ WO_3	300	10 s	2 min	99.80

of 94.81% at an optimum operating temperature (i.e. 350 °C). Upon Ru doping in WO_3, the operating temperature of the sensor got reduced to 300 °C with an improvement in the sensitivity to 98.01% due to catalytic effect. Similar observation was made in case of Pd doped WO_3, where the marginal decrement in the operating temperature (325 °C) was occurred. Surprisingly, instead of an improvement in the gas sensitivity, Pd/WO_3 sensor showed remarkable improvement in the gas response/recovery time (response in 10 s, and recovery in 2min 30sec) as compared to pristine and Ru doped WO_3 (see Table 2). It is important to highlight over here is, Ru doping led to reduction in the operating temperature and enhancement in the gas response of WO_3. On the other hand, Pd doping directed to reduce the response/recovery time, keeping the marginal decrement in the sensitivity of WO_3. The following Table 2, shows the gas sensing details of the aforementioned sensors, where critical observation can be seen. It has given the motivation to study the synergistic effect of Ru and Pd doping in the native WO_3 collectively, in order to enhance the gas sensitivity with lower operating temperature and response/recovery time. The doping of Ru and Pd in WO_3 led to the remarkable results that shown the enhancement in the gas response properties. The S% value has hit 99.80% towards 500 ppm acetone vapor at an operating temperature of 300 °C. Moreover, the response/recovery time also got reduced to 10 sec and 2 min, respectively. This tread off between the reduced response/recovery time and enhanced acetone sensitivity has been achieved using the synergistic effect of Ru and Pd in a combined manner.

It is noteworthy to mention that all the sensors showed the good sensitivity even at lower operating temperatures (200–275 °C). The pristine WO_3 at 275 °C showed the sensitivity of 89.37%, which got improved to 96.20%, upon Ru doping. Similarly, one can see that at 225 °C, the pristine WO_3 has the sensitivity of 79.09%, which had shooted to 91.15% upon synergetic effect of Ru and Pd doping in the WO_3. It clearly demonstrate the practical usability of the developed sensors even at lower operating temperatures.

Sensor response in the range of 10–1000 ppm acetone vapours for both pristine and noble metal (Ru, Pd) doped WO_3 sensors at their respective optimum operating temperature is depicted in Fig. 10. b as a function of acetone concentration. It was discovered that the graph has a tendency to grow as the acetone concentration increases up to certain value. In the beginning, the reaction climbed swiftly and eventually reached saturation level. Overall, the response of the sensor grows dramatically up to 500 ppm, beyond which the change in the sensor response is minimal and becomes plateau. In the initial phase of the graph for individual sensors, a linear relationship between sensor response and acetone concentration can be seen. This linear response can be expressed mathematically as: $S = A[C]^N + D$, where C = gas concentration, A and D are constants, and N ranging from 0.5 to 1.0 influenced by the charge of the surface species as well as the stoichiometry of the elements on the surface of the semiconductor [27]. Important to mention over here, the pristine WO_3 showed the response, barely at 10 ppm acetone concertation (S = 11.79%). The approach of nurturing the synergistic effect of Ru and Pd in the WO_3, has dramatically enhanced the sensitivity to 76.44% at barely 10 ppm acetone concentration. This particular result will undoubtedly helpful for diagnostic purpose of diabetic patients, as mentioned in the introduction section.

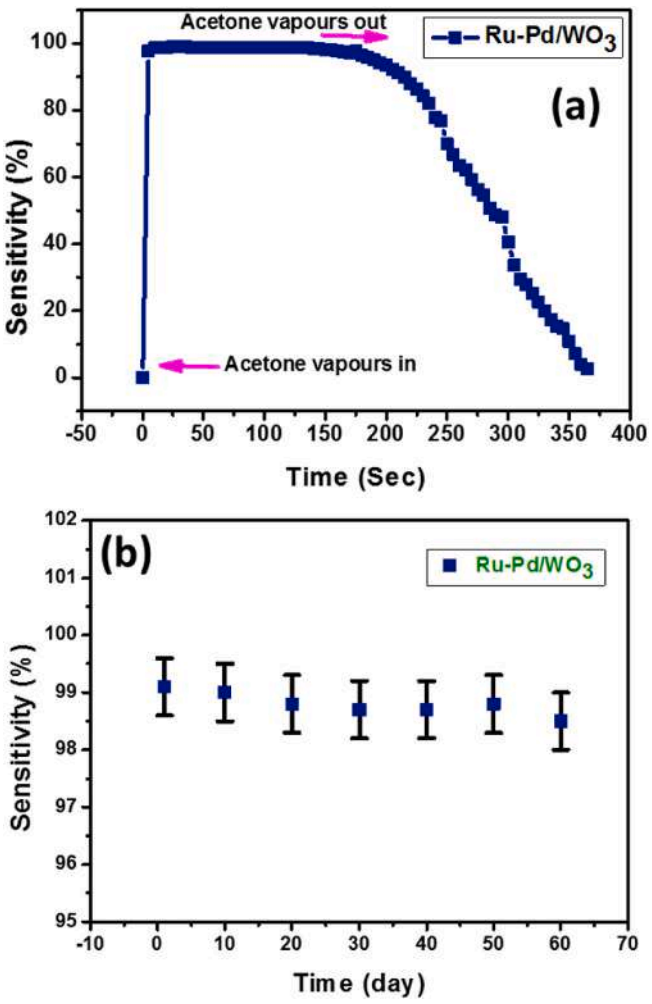

Fig. 11. a) transient response, and b) stability of Ru–Pd/WO_3 sensor.

The transient response (response/recovery behaviour) is supposed to be one of the crucial parameters of the sensor for their practical applicability. Fig. 11. a displays the transient behaviour of Ru–Pd doped WO_3 sensor at 300 °C operating temperature and 500 ppm acetone concentration. The sensor showed the quickest response of 5 s, shooting the sharp rise to 97.8% sensitivity. However, while recovery, it took 191 s with a steep slope to reach the normal condition. Fig. 11. b shows the stability of the optimised sensor (Ru–Pd/WO_3) over the period of 60 days. The sensor response was checked with the step of alternate 10 days, keeping the measurement conditions to be remained same. The sensor showed almost 98% of its initial performance after 60 days, confirming the stability of the sensor material for commercial application.

3.6.1. Gas sensing mechanism WO_3 and synergistic effect of Ru and Pd doping

The well-established oxygen ionosorption model based on conductance variation was used to study the gas sensing mechanism of WO_3. The depletion layers formed by oxygen species (viz. O_2^-, O^-, and O^{2-}) ionosorbed on the surface of WO_3 determines the gas sensing behaviour. When WO_3 is exposed to the air, the formation of depletion layers result in an increase in the potential barrier. As soon as the sensor surface (WO_3) comes in contact with the reducing gas (acetone in the present case), the electrons trapped oxygen species gets released (Fig. 12a). This conductivity change due to presence of acetone is detected, to calculate the sensitivity of developed WO_3.

In general, the parameters that determine conductivity have an impact on gas sensing capabilities. In this context, (i) the obtained WO_3 is capable of realizing good sensing properties because of its mesoporous nature. Its interconnected structure and mesopores are beneficial to the chemisorption and dissociation of oxygen species. (ii) The enhanced gas sensing mechanism due to cumulative effect of Ru and Pd doping in WO_3 nanomaterials can be explained by electronic sensitization effect of Ru and Pd. The presence of a potential barrier between the semiconductors is required for electronic sensitization. In the doping structure, noble metal oxides and WO_3 are in contact. Until the Fermi levels are equivalent, electrons would transfer from WO_3 to noble metal oxides (Fig. 12b). This process generates an electron depletion layer on the

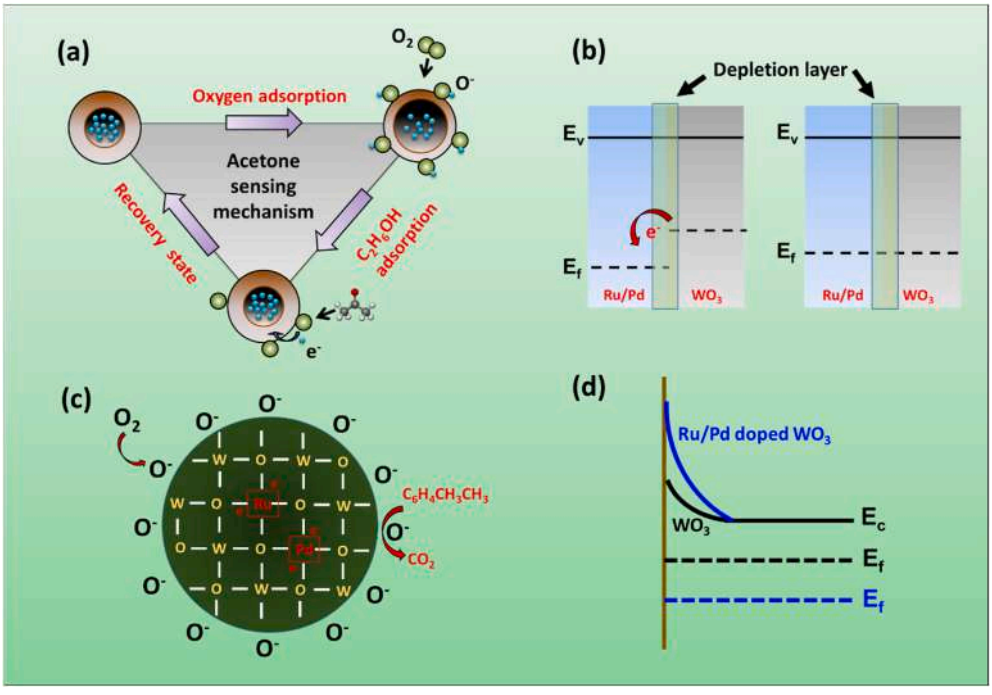

Fig. 12. a) acetone sensing mechanism of pristine WO_3, b,d) Energy band diagram of Ru/Pd doped WO_3, and c) schematic of synergistic effect due to surface defects.

surface of WO_3 and further bends the energy band, resulting in a lower resistance state and stronger gas sensing responses.

The synergistic effect of Ru and Pd doping in WO_3, towards enhancement in gas response can be described using surface defects as well. As illustrated in Fig. 12. c, the presence of the surface defects generated due to Ru and Pd doping leads to an increase in the baseline resistance and a general increase of the sensor response by acting as electron traps [28,29]. An overview of the surface as well as bulk influences of the Ru/Pd doped WO_3 compared to the pristine WO_3 material is presented in Fig. 12. d. In case of Ru/Pd addition (Blue line), a larger initial band bending can be found on the surface of the sensor material as compared with that of pristine WO_3 (Black line). The position of the Fermi level of Ru/Pd doped WO_3 lies below the Fermi level of pristine WO_3, due to the existence of surface defects acting as electron traps. This leads to an enhancement in the gas response properties of the doped material.

4. Conclusions

In conclusion, the synergistic effect of Ru and Pd noble metals on WO_3 gas response properties are systematically investigated. The sensor material was developed using facile precipitation route. XRD analysis showed the developed material is of monoclinic crystal structure. As expected in the precipitation route, the irregular grains made-up of nano-slits are observed through FESEM and TEM analyses. The Fast Fourier Transform analysis revalidated the XRD analysis confirming the major peaks (002), (020), and (200). The band gap values of pure and Pd doped WO_3 were found to be greater than Ru/WO_3 and Ru–Pd/WO_3. The nitrogen adsorption/desorption studies re-confirmed the slit-like morphology with type IV isotherm of H_3 loop. The surface area of WO_3 sensor got increased due to doping of Ru and Pd noble metals (68.39 m^2/g). The constituted elements such as W, O, Ru and Pd are confirmed using EDAX analysis as well as mapping. The XPS analysis showed the oxidation states of different elements on the surface of Ru–Pd doped WO_3. The practical usability of the developed material as a gas sensor was estimated using different target gases, where acetone has highest response. The synergetic effect of Ru and Pd has a profound influence on the gas response properties of WO_3 (S = 99.80%, and response/recovery time = 10 s and 2 min) at 300 °C operating temperature. The sensor showed decent sensitivity even at lower operating temperatures up to 200 °C. The synergistic effect of Ru and Pd in the WO_3, has dramatically tread off the sensitivity to 76.44% at barely 10 ppm acetone concentration. This particular result will undoubtedly helpful for diagnostic purpose of diabetic patients. As a consequence, considering its stability of ~98% over the span of 60 days, high sensitivity (99.80%), and fast response/recovery (10 s, 2 min), the developed sensor is a potential candidate for the practical acetone sensor.

Declaration of competing interest

The authors declare that they have no known competing financial interests or personal relationships that could have appeared to influence the work reported in this paper.

Acknowledgments

Dr. Digambar Nadargi acknowledges UGC Dr. D. S. Kothari Postdoctoral Fellowship Scheme, India for awarding Post Doctoral Fellowship (No. F.42/2006(BSR)/PH/19–20/0013). Dr. J. S. Park would like to acknowledge National Research Foundation (NRF), Korea for the research grant (NRF. 2020R1I1A3070554).

Appendix A. Supplementary data

Supplementary data to this article can be found online at https://doi.org/10.1016/j.ceramint.2022.03.065.

References

[1] S. Padamata, A. Yasinskiy, P. Polyakov, E. Pavlov, D. Varyukhin, Recovery of noble metals from spent catalysts: a Review, Metall. Mater. Trans. B 51 (2020) 2413.
[2] J. Ou, M. Yaacob, M. Breedon, H. Zheng, J. Campbell, K. Latham, J. Plessis, W. Wlodarski, K. Kalantar-zadeh, In situ Raman spectroscopy of H_2 interaction with WO_3 films, Phys. Chem. Chem. Phys. 13 (2011) 7330.
[3] R. Charles, P. Douglas, I. Hallin, I. Matthews, G. Liversage, An investigation of trends in precious metal and copper content of RAM modules in WEEE: implications for long term recycling potential, Waste Manag. 60 (2017) 505.
[4] F. Xiu, F. Zhang, Size-controlled preparation of Cu_2O nanoparticles from waste printed circuit boards by supercritical water combined with electrokinetic process, J. Hazard Mater. (2012) 200.
[5] S. Abdelbasir, K. McCourt, C. Lee, D. Vanegas, Waste-Derived Nanoparticles: synthesis approaches, environmental applications, and sustainability considerations, Front. Chem. 8 (2020) 782.
[6] S. Kochuveedu, Y. Jang, D. Kim, A study on the mechanism for the interaction of light with noble metal-metal oxide semiconductor nanostructures for various photophysical applications, Chem. Soc. Rev. 42 (2013) 8467.
[7] F. Nosheen, T. Anwar, A. Siddique, N. Hussain, Noble metal based alloy nanoframes: syntheses and applications in fuel cells, Front. Chem. 7 (2019) 456.
[8] M. Barbosa, P. Suman, J. Kim, H. Tuller, J. Varela, M. Orlandi, Gas sensor properties of Ag and Pd-decorated SnO micro-disks to NO_2, H_2 and CO: catalyst enhanced sensor response and selectivity, Sensor. Actuator. B Chem. 239 (2017) 253.
[9] V. Chaudhary, I. Mulla, K. Vijayamohanan, Comparative studies of doped and surface modified tin oxide towards hydrogen sensing: synergistic effects of Pd and Ru, Sensor. Actuator. B 50 (1998) 45.
[10] F. Zheng, L. Zhang, Y. Li, Qingchao Liu, Zhongjun Li, H. Yao, Bimetallic AuPd alloy nanoparticles decorated on macroporous WO_3 supports for selective detection of acetone, ACS Appl. Nano Mater. 4 (2021) 2713.
[11] J. Li, Q. Zhou, Z. Shen, S. Li, J. Pu, C. Zhong, M. Cao, X. Jin, H. Zhang, Y. Wang, H. Ma, Synergistic effect of ultrafine nano-Ru decorated cobalt carbonate hydroxides nanowires for accelerated alkaline hydrogen evolution reaction, Electrochim. Acta 331 (2019), 135367.
[12] S. Mehta, D. Nadargi, M. Tamboli, T. Alshahrani, V. Reddy, E. Kim, I. Mulla, C. Park, S. Suryavanshi, RGO/WO_3 hierarchical architectures for improved H_2S sensing and highly efficient solar-driving photo-degradation of RhB dye, Sci. Rep. 11 (2021) 5023.
[13] Y. Li, Z. Hua, Y. Wu, Y. Zeng, Z. Qiu, X. Tian, M. Wang, E. Li, Modified impregnation synthesis of Ru-loaded WO_3 nanoparticles for acetone sensing, Sensor. Actuator. B 265 (2018) 249.
[14] H. Xu, J. Gao, M. Li, Y. Zhao, M. Zhang, T. Zhao, L. Wang, W. Jiang, G. Zhu, X. Qian, Y. Fan, J. Yang, W. Luo, Mesoporous WO_3 nanofibers with crystalline framework for high-performance acetone sensing, Front. Chem. 7 (2019) 266.
[15] Y. Li, Z. Hua, Y. Wu, Y. Zeng, Z. Qiu, X. Tian, Mengjun Wang, Erping Li Modified impregnation synthesis of Ru-loaded WO_3 nanoparticles for acetone sensing, Sensor. Actuator. B 265 (2018) 249.
[16] P. Gao, H. Ji, Y. Zhou, X. Li, Selective acetone gas sensors using porous WO_3–Cr_2O_3 thin films prepared by Sol–gel method, Thin Solid Films 520 (2012) 3100.
[17] J. Meng, J. Pei, Z. He, S. Wu, Q. Lin, X. Wei, J. Li, Z. Zhang, Facile synthesis of g-C_3N_4 nanosheets loaded with WO_3 nanoparticles with enhanced photocatalytic performance under visible light irradiation, RSC Adv. 7 (2017), 24097.
[18] N. Li, Y. Zheng, L. Wei, H. Teng, J. Zhou, Ruthenium nanoparticles decorated tungsten oxide as a bifunctional catalyst for electrocatalytic and catalytic applications, Green Chem. 19 (2017) 682.
[19] Y. Fujioka, J. Frantti, A. Asiri, A. Obaid, H. Jiang, R. Nieminen, Structural properties of pure and nickel-modified nanocrystalline tungsten trioxide, J. Phys. Chem. C 116 (2012), 17029.
[20] Y. Fujioka, J. Frantti, R. Nieminen, A. Asiri, Formation of ruthenium cluster on nanocrystalline tungsten trioxide, J. Phys. Chem. C 117 (2013) 7506.
[21] M. Sun, N. Xu, Y. Cao, J. Yao, E. Wang, Ultraviolet-visible emission from three-dimensional WO 3−x nanowire networks, J. Mater. Res. 15 (2000) 927.
[22] S. Ghosh, S. Acharyya, M. Kumar, R. Bal, Chloride promoted room temperature preparation of silver nanoparticles on two dimensional tungsten oxide nano architectures for the catalytic oxidation of tertiary N-compounds to N-Oxides, Nanoscale 7 (2015) 15197.
[23] M. Hubner, D. Koziej, J.-D. Grunwaldt, U. Weimar, N. Barsan, An Au clusters related spill-over sensitization mechanism in SnO_2 based gas sensors identified by operando HERFD-XAS, work function changes, DC resistance and catalytic conversion studies, Physiol. Chem. Phys. 14 (2012), 13249.
[24] S. Mehta, D. Nadargi, M. Tamboli, V. Patil, I. Mulla, S. Suryavanshi, W. O.3 Macroporous, Tunable morphology as a function of glycine concentration and its excellent acetone sensing performance, Ceram. Int. 45 (2019) 409.
[25] N. Duy, N. Hieu, P. Huy, N. Chien, M. Thamilselvan, J. Yi, Mixed SnO_2/TiO_2 Included with carbon nanotubes for gas sensing application, Physica E 41 (2008) 258.
[26] Z. Jing, J. Zhan, Fabrication and gas-sensing properties of porous ZnO nanoplates, Adv. Mater. 20 (2008) 4547.

[27] F. Shaikh, L. Chikhale, I. Mulla, S. Suryavanshi, Synthesis and enhanced ethanol sensing performance of nanostructured Sr doped SnO_2 thick film sensor, J. Mater. Sci. Mater. Electron. 28 (2017) 4.
[28] M. Hübner, N. Bârsan, U. Weimar, Influences of Al, Pd and Pt additives on the conduction mechanism as well as the surface and bulk properties of SnO_2 based polycrystalline thick film gas sensors, Sens. Actuators, B 171 (2012) 172.
[29] F. Li, Q. Qin, N. Zhang, C. Chen, L. Sun, X. Liu, Y. Chen, C. Li, S. Ruan, Improved gas sensing performance with Pd-doped $WO_3{\cdot}H_2O$ nanomaterials for the detection of xylene, Sens. Actuators, B 244 (2017) 837.